THE JOURNAL OF PHYSICAL CHEMISTRY C

Article

pubs.acs.org/JPCC

Effect of Electrolytes on the Selectivity and Stability of n-type WO_3 Photoelectrodes for Use in Solar Water Oxidation

James C. Hill and Kyoung-Shin Choi*

Department of Chemistry, Purdue University, West Lafayette, Indiana 47907, United States

Supporting Information

ABSTRACT: High surface area porous n-type WO_3 electrodes were prepared electrochemically and used as a photoanode in a water-splitting photoelectrochemical cell. Various electrolytes containing different anions (acetate, chloride, phosphate, perchlorate, and sulfate) and cations (Li^+, Na^+, and K^+) were prepared at pH 1, 3, and 5 to investigate how these anions and cations affect the efficiency of the photo-oxidation reaction of water on the WO_3 surface. To quantitatively compare their effects on O_2 evolution, photocurrent to oxygen conversion efficiency was obtained for each electrolyte by simultaneously measuring photocurrent and O_2 produced in a sealed divided cell. The type of competing reactions present in each electrolyte and their effects on water oxidation to O_2 or to hydrogen peroxide, which is known to accumulate on the WO_3 surface and cause photocorrosion, were investigated. The results reported in this study will be useful in formulating optimum electrolyte compositions to enhance desired photo-oxidation reactions for various photoelectrochemical cells.

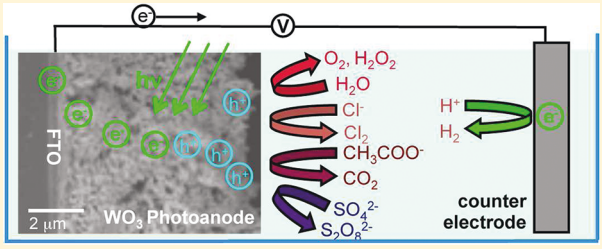

INTRODUCTION

Tungsten trioxide (WO_3) is an n-type semiconductor that has a bandgap energy of ca. 2.6 eV. It has been investigated as a photoanode for the photoelectrolysis of water, because it is inexpensive, environmentally benign, and chemically stable in acidic to semiacidic aqueous media (pH < 7).[1−19] In a water-splitting photoelectrochemical cell, photogenerated holes in the valence band of an n-type WO_3 electrode are used at the WO_3/electrolyte junction to oxidize water to O_2 while photoexcited electrons in the conduction band are moved to the counter electrode to reduce protons to H_2. (An external bias is necessary to complete the H_2 evolution reaction as the conduction band edge and flatband potential of WO_3 are not located at a negative enough potential to reduce protons.) However, previous studies on n-type WO_3 electrodes reported that oxidation of water to O_2 was not the only photo-oxidation reaction that occurred at the WO_3 surface under illumination (eq 1).[18−20] Because of poor kinetics at the WO_3 surface for the O_2 evolution reaction, incomplete oxidation of water to peroxide species can also easily occur (eq 2). The formation and accumulation of peroxide species on the WO_3 surface were reported to cause considerable decreases in photocurrent over time and eventually resulted in the photoinactivity of the WO_3 surface,[18,19] which warranted recent studies seeking various ways to enhance the photostability of WO_3.[19,21,22] In addition, photo-oxidation of anions in the solution present as supporting electrolytes (e.g., Cl^-, SO_4^{2-}) can also compete with the photo-oxidation of water (eqs 3,4).[18,20,23,24]

$$2H_2O \rightarrow 4H^+ O_2 + 4e^- \quad E^o = 1.228\text{V vs NHE} \qquad (1)$$

$$2H_2O \rightarrow 2H^+ + H_2O_2 + 2e^- \quad E^o = 1.776\text{V vs NHE} \qquad (2)$$

$$2Cl^- \rightarrow Cl_2 + 2e^- \quad E^o = 1.358\text{V vs NHE} \qquad (3)$$

$$2SO_4^{2-} \rightarrow S_2O_8^{2-} + 2e^- \quad E^o = 2.010\text{V vs NHE} \qquad (4)$$

These competing reactions are thermodynamically less favorable than the oxidation of water to O_2.[20,23,24] Therefore, they are of no serious concern for the electrolysis of water in the dark. However, for photo-oxidation achieved by photogenerated holes in a photoanode, these reactions can compete with water oxidation if holes in the valence band edge of the photoanode have enough overpotential to drive these reactions, which is the case for WO_3.[19] (The valence band edge of WO_3 is located at ca. 2.97 V vs NHE at pH = 0).[25] In particular, if the kinetics of O_2 evolution on the photoanode surface is poor, these competing reactions can consume the majority of photogenerated holes, significantly decreasing the O_2 evolution efficiency. Therefore, a systematic investigation on the effects of electrolytes (anions, cations, pH) on oxygen evolution and peroxo formation would be extremely beneficial for formulating conditions, which minimize undesirable side reactions and maximize long-term stability for WO_3 photoanodes and for any other photoanode in general.

In this study, we prepared acetate, chloride, phosphate, perchlorate, and sulfate solutions with varying pH's (pH 1, 3, and 5) and studied the effect of each anion on the photo-oxidation of water on the WO_3 photoanode in a quantitative

Received: October 14, 2011
Revised: March 14, 2012
Published: April 2, 2012

   dx.doi.org/10.1021/jp209909b | J. Phys. Chem. C 2012, 116, 7612−7620

manner for the first time. We also changed cationic types (Li^+, Na^+, and K^+) to probe whether cations also exert any noticeable effect on the photo-oxidation of water. WO_3 electrodes used in this study were prepared by electrodeposition. We report new deposition conditions modified from those previously established,[26−29] which produce highly porous WO_3 electrodes that generate significantly enhanced photocurrents. As a result, more reliable photocurrent measurement and O_2 detection were possible. Simultaneous measurements of photocurrent and O_2 were carried out using a sealed divided cell to analyze what portion of the photocurrent was associated with water oxidation to O_2 in each electrolyte (i.e., photocurrent to oxygen conversion efficiency). Because of its poor kinetics for O_2 evolution, the WO_3 surface provided an ideal system to examine all possible photo-oxidation reactions that can compete with photo-oxidation of water. Here, we report the synthesis of a porous WO_3 electrode and the effects of various cations and anions on the photoelectrochemical performance and the stability of WO_3 electrodes for use as a photoanode in a water-splitting photoelectrochemical cell.

EXPERIMENTAL SECTION

Synthesis of WO_3. The plating solution was prepared by dissolving tungsten metal powder (99.95%, <1 μm, Alfa Aesar) in excess hydrogen peroxide solution (30%, ACS, Mallinckrodt) to produce a 0.1 M peroxo-tungstic acid solution.[27,29] The dissolution process was very exothermic and resulted in a colorless solution. Subsequently, the excess hydrogen peroxide was decomposed with platinum black (Alfa Aesar). After the cessation of effervescence, the appropriate amounts of high purity water (Millipore Milli-Q purified system, resistivity ≥18 MΩ) and alcohol, either isopropyl alcohol (IPA, reagent grade, Mallinckrodt) or ethylene glycol (EG, purified, Spectrum), were added while stirring. The resulting peroxo-tungstic acid solution had a pH of ca. 1.3. Electrodeposition was carried out in an undivided cell using a three-electrode setup consisting of an Ag/AgCl (4 M KCl) reference electrode, fluorine-doped tin oxide (FTO) (8−12 Ω resistance) as the working electrode, and a glass slide sputter coated with 1000 Å of platinum on 300 Å of titanium as the counter electrode. All potential values reported in this study are against the Ag/AgCl (4 M KCl) reference electrode. Prior to use, FTO was soaked in 2 wt % Alconox solution at 95 °C for 5 min, then sonicated and rinsed with isopropyl alcohol and DI water. Tungsten oxide films were deposited potentiostatically at E = −600 mV vs Ag/AgCl using a VMP2 multichannel potentiostat (Princeton Applied Research). The resulting blue films were washed with DI water and dried under nitrogen. The as-deposited amorphous films were converted to crystalline WO_3 electrodes by annealing at 500 °C for 1 h in air, with a 2 °C/min ramping rate.

Characterization. Powder X-ray diffraction (XRD) patterns were collected using a Scintag X2 diffractometer (Cu K_α radiation). UV−vis absorption spectra were measured with a Cary 300 UV−vis spectrophotometer in diffuse reflectance mode by scraping tungsten oxide films off the FTO substrate it had been deposited on and mounting the resulting powders onto the compact barium sulfate matrix that was used as the reference (Fisher Scientific). Scanning electron microscopy (SEM) images were acquired via a field emission scanning electron microscope (FEI Nova NanoSEM) at an accelerating voltage of 5 kV. The SEM samples were first sputter coated with ca. 2 nm thick Pt.

Electrolyte Preparation for Photocurrent Measurements. The acetate solution (pH 5) was prepared by adjusting the pH of a 0.1 M CH_3COONa solution (as-prepared solution, pH 8.2) with acetic acid. The final concentration of acetate and acetic acid in solution ($[CH_3COO^- + CH_3COOH]$) was 0.16 M. The acetate solution (pH 3) was prepared by adjusting the pH of a 0.1 M acetic acid solution (as-prepared pH, 2.7) with NaOH. The sodium chloride solutions (pH 1, 3, and 5) were prepared by adjusting the pH of a 0.1 M NaCl solution (as-prepared solution, pH 5.1) with HCl. This procedure increased the final concentration of Cl^- ions in the pH 1 solution to 0.19 M, but the change of the sodium concentration was negligible. The sodium perchlorate solutions (pH 1, 3, and 5) were prepared by adjusting the pH of a 0.1 M $NaClO_4$ solution (as-prepared solution, pH 5.8) with $HClO_4$. This procedure increased the final concentration of ClO_4^- ions in the pH 1 solution to 0.17 M, but the change of the sodium concentration was negligible. The sodium phosphate solution (pH 5) was prepared by adjusting the pH of a 0.1 M NaH_2PO_4 solution (as-prepared solution, pH 4.3) with NaOH, while the sodium phosphate solutions (pH 1 and 3) were prepared by adjusting the pH of a 0.1 M NaH_2PO_4 solution with H_3PO_4. Because the pK_{a1} of H_3PO_4 is only 2.148, a significant amount of H_3PO_4 was necessary to lower the pH to 1, and the final concentration of phosphate in the pH 1 solution was 0.81 M. The change of the sodium concentration was negligible. The sulfate solutions (pH 1, 3, and 5) were prepared by adjusting the pH of a 0.1 M Na_2SO_4 solution (as-prepared solution, pH 5.7) with sulfuric acid. This procedure increased the final concentration of sulfate in the pH 1 solution to 0.17 M, but the change of the sodium concentration was negligible. The sulfate, phosphate, and perchlorate solutions (pH 3) containing lithium and potassium ions were prepared by the same procedure using the corresponding compounds containing lithium and potassium ions.

Photocurrent Measurements. Photocurrent measurements utilized simulated solar illumination obtained by passing light from a 300 W xenon arc lamp through neutral density filters and an AM 1.5G filter into an optical fiber and calibrating the output to 100 mW/cm^2 at the WO_3 film surface (front illumination). The illuminated area was 0.2 cm^2. The linear sweep voltammograms (LSVs) were obtained by scanning in the negative direction at a scan rate of 10 mV/s with chopped illumination (AM 1.5G, 100 mW/cm^2) to obtain photocurrent and dark current using a single sweep. When photocurrent and O_2 measurements (see below for details) were carried out simultaneously, the light intensity was increased to 400 mW/cm^2 to ensure a higher signal-to-noise ratio in O_2 measurement because O_2 generated from the limited illuminated area, 0.2 cm^2, in our measurement setup was not substantial when the standard illumination was used. All electrolytes were purged with Ar before photocurrent measurement. The electrochemical cell consisted of the aforementioned prepared n-WO_3 film was used as the working electrode (photoanode), a glass slide sputter coated with 1000 Å of platinum on 300 Å of titanium as the counter electrode, and an Ag/AgCl (4 M KCl) reference electrode. A constant potential of 0.9 V vs Ag/AgCl was applied to all samples during photocurrent and oxygen detection measurements.

Oxygen Detection. Oxygen was detected quantitatively using an Ocean Optics fluorescence-based oxygen sensor (FOSPOR-R 1/16"). A custom-built airtight two-compartment cell divided by a frit was used for simultaneous measurements

dx.doi.org/10.1021/jp209909b | J. Phys. Chem. C 2012, 116, 7612−7620

of photocurrent and O_2. One side held a Pt counter electrode, while the other side held the WO_3 photoanode along with an Ag/AgCl reference electrode. Both sides of the split cell were filled with 30 mL of electrolyte, which left approximately 15 mL of headspace. The solution and headspace were purged with argon prior to capping the cell. The compartment was not completely oxygen leak proof; thus the leak rate was determined and subtracted from the experimental data by calculating the slope of the baseline before and after photoelectrochemically oxidizing the photoelectrolyte solution. The needle probe of the oxygen sensor was inserted into a septum on the cap of the WO_3 compartment. A two-point calibration was performed using argon as 0% O_2 and air as 20.9% O_2. The probe measures the O_2 content in the headspace and records it as mole %. This was converted to mmol after first adjusting for the O_2 dissolved in solution using Henry's Law. The expected amount of O_2 was calculated from the total charge passed as photocurrent during illumination assuming 100% Faradaic efficiency for O_2 production. The photocurrent to O_2 conversion efficiency, the measure of what portion of the photocurrent was associated with O_2 production, was obtained using the following equation (eq 5):

$$\text{photocurrent to } O_2 \text{ conversion efficiency}(\%) = \frac{\text{actual amount of } O_2 \text{ detected}}{\text{expected amount of } O_2 \text{ produced based on photocurrent}} \times 100\% \quad (5)$$

Gas Chromatography (GC) Analysis. Gas chromatography (GC) was used to confirm photo-oxidation products when 0.1 M sodium acetate solution (pH 5) was used for the photoelectrolysis of water by a WO_3 photoanode. An SRI 8610C GC was used with a HayeSepD stainless steel packed column. High-purity helium (Indiana Oxygen, 99.999%) was used as the carrier gas, and a helium ionization detector (HID) was used. 0.5 mL of the sample was taken from the head space of the sealed cell after illuminating 0.2 cm^2 of a WO_3 photoanode at 0.9 V vs Ag/AgCl (light intensity: 400 mW/cm^2 with an AM 1.5G filter, total charge passed as photocurrent = 3.2 C), and the sample was injected directly onto the column.

Cl_2 Detection. Cl_2 produced by photo-oxidation of Cl^- in the chloride solutions was detected by the iodide–starch test ($Cl_2 + I^- \rightarrow I_2 + Cl^-$). Chlorine produced in the presence of iodide acted as an oxidizing agent and oxidized iodide to iodine while being reduced to chloride. The resulting iodine was quantified by titrating with sodium thiosulfate using starch as a color indicator ($I_2 + 2S_2O_3^{2-} \rightarrow 2I^- + S_4O_6^{2-}$). For this experiment, 30 mL of 100 mM sodium chloride solution was prepared and used as an electrolyte for a WO_3 photoanode illuminated for 1 h (400 mW/cm^2 with an AM 1.5G filter) while applying 0.9 V vs Ag/AgCl. The total charge passed through as photocurrent could produce 10.2 μmol of Cl_2 when 100% Faradaic efficiency is assumed. To this solution, potassium iodide was added to the concetration of 50 mM. Three milliliters of the resulting solution was titrated with 0.1 mL of 10 mM sodium thiosulfate solution. This result indicated that the majority of the photocurrent (>95%) was used for chloride oxidation.

RESULTS AND DISCUSSION

The plating solution used for the deposition of WO_3 contained tungsten(VI) peroxo species, $W_2O_{11}^{2-}$ (i.e., $[W_2(O_2^{2-})_4(O^{2-})_3]^{2-}$), which were obtained by dissolving tungsten metal in hydrogen peroxide. An amorphous hydrated form of WO_3 film was cathodically deposited on the working electrode when these species were decomposed by the reduction of peroxo groups as shown in eq 6.[29]

$$W_2O_{11}^{2-} + 10H^+ + nH_2O + 8e^- \rightarrow 2WO_3 \cdot nH_2O + 5H_2O \quad (6)$$

The color of the as-deposited film was blue, but it gradually disappeared when the film was exposed to air. The blue color suggests the presence of tungsten(V) ions in the as-deposited film (e.g., hydrated form of H_xWO_3, WO_{3-x}, or H_xWO_{3-y}) with the color originating from d–d transitions. It seems that during the reduction of peroxide (E = −0.6 V vs Ag/AgCl), some W(VI) ions in the WO_3 film were also partially reduced to W(V). The as-deposited film was converted to a crystalline WO_3 film (space group: $P2_1/n$, PDF no: 43-1035) by annealing at 500 °C in the air, which was confirmed by X-ray diffraction (Supporting Information). The color of the fully oxidized WO_3 film was light opaque yellow. Its bandgap was estimated to be 2.6 eV based on its UV–vis spectrum (Supporting Information).

The tungsten peroxo species present in the plating solution are not very stable and form a precipitate within a few hours of preparation. Therefore, isopropanol (IPA) was typically added as a stabilizer in previous studies.[27,29] However, the relatively low boiling point of IPA (82.5 °C) makes it difficult to maintain a constant concentration when the deposition is carried out at an elevated temperature. Therefore, in this study, we replaced IPA with ethylene glycol (EG), which has a higher boiling point (197.6 °C), to study the effect of deposition temperature on the electrodeposition of WO_3 films and investigate whether the presence of EG and elevated deposition temperatures affect the morphology and photoelectrochemical properties of the resulting WO_3 electrodes.

Figure 1a,b compares SEM images of WO_3 films deposited with 25 vol % IPA and 25 vol % EG at room temperature. The use of IPA resulted in the formation of a WO_3 electrode with a flat and featureless two-dimensional surface, but the use of EG created a film with a rough and porous surface. The porosity increased further when the amount of EG increased from 25 to 50 vol % (Figure 1c). As the content of EG increased, the plating medium became more viscous and hindered facile ion diffusion, which appeared to trigger diffusion-limited growth more easily and resulted in the deposition of high surface area films with a porous morphology. When the deposition temperature of the plating solution containing 50 vol % EG was raised to 45 °C, the resulting enhanced deposition kinetics created a more severe diffusion limited growth, and, therefore, a film with a even higher porosity and surface area was obtained (Figure 1d). Because of the enhanced porosity and the resulting volume expansion, the film deposited from a 45 °C solution containing 50 vol % EG is approximately 6 times thicker than the film deposited from room temperature solution containing 25 vol % IPA despite being deposited by passing the same amount of charge, 0.72 C (Figure 1e,f). These results show that the use of EG had a distinct advantage in generating high surface area porous morphologies while allowing for more reproducible deposition of WO_3 electrodes at an elevated temperature.

Figure 2 shows photocurrent obtained from the four WO_3 electrodes shown in Figure 1a–d under AM 1.5G, 100 mW/cm^2 illumination at 0.9 V vs Ag/AgCl in a 0.1 M sodium acetate

dx.doi.org/10.1021/jp209909b | J. Phys. Chem. C 2012, 116, 7612–7620

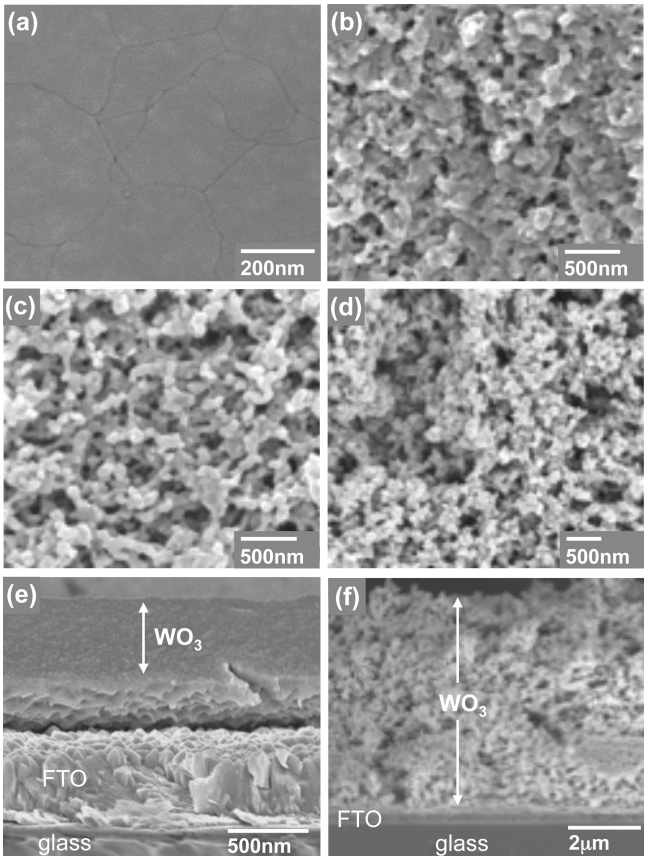

Figure 1. SEM images of WO_3 electrodes deposited with (a) 25 vol % IPA at room temperature, (b) 25 vol % EG at room temperature, (c) 50 vol % EG at room temperature, and (d) 50 vol % EG at 45 °C. Parts (e) and (f) show the side view SEM images of (a) and (d), respectively. (The same amount of charge, 0.72 C, was used to deposit WO_3 electrodes shown here.)

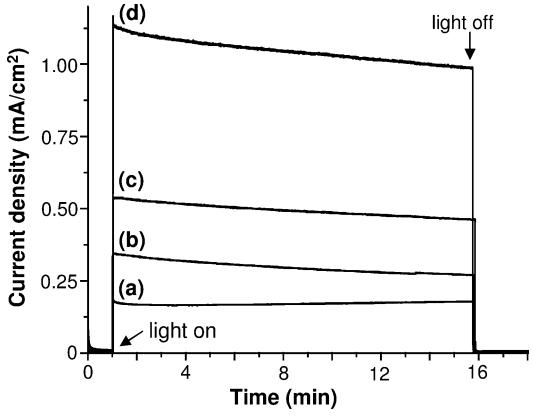

Figure 2. Photocurrent of WO_3 electrodes deposited with (a) 25 vol % IPA at room temperature, (b) 25 vol % EG at room temperature, (c) 50 vol % EG at room temperature, and (d) 50 vol % EG at 45 °C obtained at 0.9 V vs Ag/AgCl in 0.1 M sodium acetate solution with pH adjusted to 5 under AM 1.5G, 100 mW/cm^2 illumination.

solution with pH adjusted to 5. All electrodes commonly generated anodic photocurrents, confirming that they are n-type and serve as photoanodes conducting photo-oxidation reactions at the surface under illumination. Figure 2 also shows that the porosity and the surface area of the WO_3 electrodes have a direct impact on photocurrent, and the WO_3 electrode deposited with 50 vol % EG at 45 °C, which had the highest surface area, generated the highest photocurrent. When the EG content was increased above 50 vol % or deposition temperature above 45 °C, no additional increase in surface area or photocurrent was observed. Therefore, WO_3 electrodes deposited with 50 vol % EG at 45 °C were used for the remainder of this study to investigate the effect of various electrolytes on the photo-oxidation of water.

Acetate Solution. Photocurrent of WO_3 was measured in a 0.1 M acetic acid solution with pH adjusted to 3 and a 0.1 M sodium acetate solution with pH adjusted to pH 5. An acetate solution with pH lower than 3 was not investigated because it requires the addition of a stronger acid, which results in the introduction of another type of anion to the solution. Photocurrent generated by the WO_3 electrode immersed in the acetic acid solution (pH 3) is shown in Figure 3a(i). While the amount of photocurrent was significant, the O_2 detection experiment showed that none of this photocurrent was associated with the production of O_2. GC analysis identified CO_2 and ethane as the main products (Supporting Information), suggesting that the dominant photo-oxidation reaction in this solution was the oxidation of acetate ions to carbon dioxide and ethane, called the Kolbe reaction (eq 7), and the complete oxidation of acetate to carbon dioxide (eq 8).[30−34]

$$2CH_3COO^- \rightarrow C_2H_6 + 2CO_2 + 2e^- \quad (7)$$

$$CH_3COO^- + 2H_2O \rightarrow 2CO_2 + 4H^+ + 8e^- \quad (8)$$

The oxidation reactions of acetate (ca. 2.20 V vs NHE) are thermodynamically less favorable than oxidation of water to O_2.[31,32] Therefore, these reactions would not compete with the

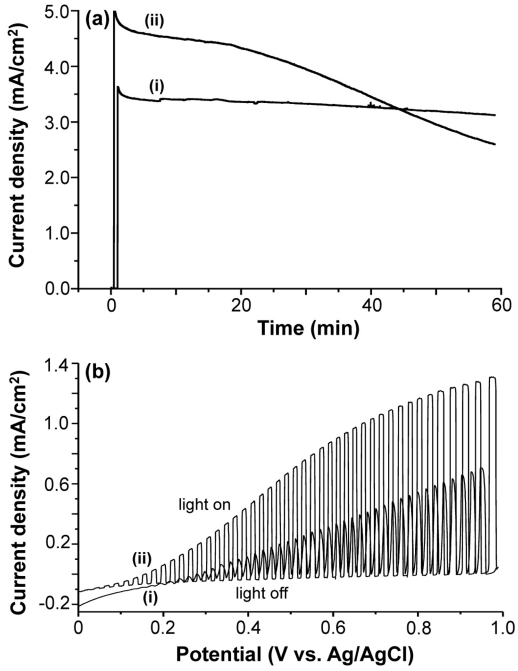

Figure 3. (a) Photocurrent of a WO_3 photoanode obtained at 0.9 V vs Ag/AgCl under 400 mW/cm^2 illumination with an AM 1.5G filter. (b) LSVs of a WO_3 obtained with chopped illumination (100 mW/cm^2 with an AM 1.5G filter, 10 mV/s) in (i) 0.1 M acetic acid solution with pH adjusted to 3 and (ii) 0.1 M sodium acetate solution with pH adjusted to pH 5.

dx.doi.org/10.1021/jp209909b | J. Phys. Chem. C 2012, 116, 7612−7620

water oxidation reaction when water is electrochemically oxidized using a potential that provides a sufficient overpotential for water oxidation but not for acetate oxidation. However, for photo-oxidation reactions, because the photogenerated holes in the valence band edge of WO_3 have enough overpotential to drive oxidation of both water and acetate,[25] the kinetically faster acetate reaction can become the dominant reaction and completely suppress the kinetically slower water oxidation reaction. In fact, it has been reported that electrolysis in the dark at sufficiently high overpotentials, which allow for both water oxidation and the Kolbe reaction, caused the efficiency of the Kolbe reaction to approach 100%.[31] This suggests that the products obtained from photo-oxidation utilizing holes at the very positive valence band edge of the WO_3 electrode are similar to those obtained from dark oxidation at the very high overpotential region.

When the pH 5 acetate solution was used, a higher initial photocurrent was observed, but the photocurrent was not stable and began to slowly decay over time (Figure 3a(ii)). Again, the O_2 detection experiment showed that no portion of the photocurrent was due to water oxidation to O_2. However, the photocurrent decay over time (Figure 3a(ii)) indicates that some portion of photocurrent generated in a pH 5 acetate solution was associated with incomplete water oxidation to peroxo species. Accumulation of peroxo species on the WO_3 surface is known to cause a gradual photocurrent decay.[18,19] Because the photocurrent obtained in the pH 3 solution was mostly stable with little sign of decay, the relative rate of peroxide formation as compared to the rate of acetate oxidation appears to diminish with decreasing pH.

The current−potential characteristics measured with chopped illumination using an identital WO_3 electrode in pH 3 and 5 acetate solutions are shown in Figure 3b. The photocurrent onset potential obtained at pH 5 (0.02 V vs Ag/AgCl) was shifted to the negative direction as compared to that otained at pH 3 (0.14 V vs Ag/AgCl). This is because the flatband potential of an ideally behaving oxide electrode shifts 59 mV to the negative direction when pH is raised by 1. This means that when the same bias is applied to WO_3 electrodes immersed in pH 3 and pH 5 solutions, the one in pH 5 solution would generate a stronger electric field (i.e., band bending) and, therefore, generate a higher photocurrent. This was originally thought to be the reason the initial photocurrent (i.e., before the photocurrent decay starts) obtained at pH 5 at 0.9 V vs Ag/AgCl shown in Figure 3a was much higher than that obtained at pH 3 at 0.9 V vs Ag/AgCl. However, Figure 3b shows that the current−potential profile obtained at pH 5 cannot be obtained by simply shifting the profile obtained at pH 3 by 118 mV in the negative direction and that the significantly enhanced photocurrent obtained at pH 5 cannot solely be explained by the pH-dependent flatband potential shift. One plausible factor that may be responsible for the observed phenomenon is the adsorption of acetic acid/acetate ions on the WO_3 surface. When the solution pH changes, the acetic acid:acetate ratio and therefore their adsorption behaviors will change, and this in turn may affect the kinetics of acetate oxidation and water oxidation significantly, creating a difference in photocurrent that cannot be explained by a simple Nernstian shift.

Chloride Solution. 0.1 M sodium chloride solutions were prepared, and the pH was adjusted to 1, 3, and 5 to operate the WO_3 photoanode. The current−potential characteristics measured with chopped illumination using an identical WO_3 electrode in these solutions are shown in Figure 4a. The

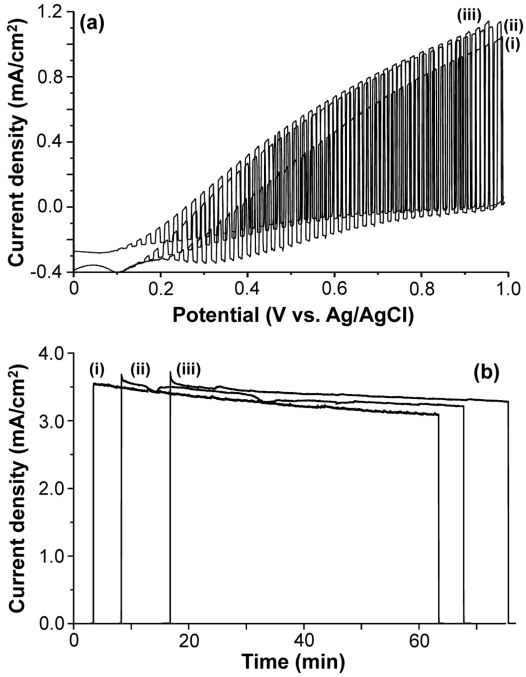

Figure 4. (a) LSVs of a WO_3 obtained with chopped illumination (100 mW/cm^2 with an AM 1.5G filter, 10 mV/s) and (b) photocurrent of a WO_3 photoanode obtained at 0.9 V vs Ag/AgCl under 400 mW/cm^2 illumination with an AM 1.5G filter in 0.1 M NaCl solution with pH adjusted to (i) 1, (ii) 3, and (iii) 5.

potential was swept to the negative direction. The dark cathodic peak observed at 0.32 V in pH 1 solution and 0.10 V in pH 3 solution are due to the electrochemical reduction of Cl_2 generated by photo-oxidation of Cl^- ions at a more positive bias region (eq 3). A shift of the photocurrent onset potential due to the pH-dependent shift of the flatband potential is again observed in these solutions. As a result, in the low bias region ($E \leq 0.3$ V vs Ag/AgCl), the amount of photocurrent generated at a given bias increases as the pH increases. However, at a higher bias region ($E \geq 0.9$ V vs Ag/AgCl) where electron−hole pairs can be easily separated, photocurrent becomes mainly limited by photon absorption and does not change drastically by the applied potential or the strength of the electric field generated. As a result, photocurrents obtained from three different pH conditions at a given bias become very similar. For example, at E = 0.9 V vs Ag/AgCl, the photocurrents obtained in pH 3 and 5 solutions are comparable, and photocurrent obtained in pH 1 solution is only slightly lower (ca. 92%). This phenomenon was commonly observed for all other electrolytes discussed below.

Figure 4b shows photocurrent−time profiles obtained at a fixed potential of 0.9 V in the three different pH conditions. For these experiments, to compare the photostability of WO_3 electrodes in a more straightforward manner, three WO_3 electrodes that generate very similar initial photocurrent in pH 1, 3, and 5 solutions at 0.9 V vs Ag/AgCl were chosen. (The same procedure was used for measuring photocurrent−time profiles in phosphate, perchlorate, and sulfate solutions discussed below.) The result shows that the photocurrents generated in these solutions are relatively stable and decay very slowly over time. However, as in the case of acetate solutions, no oxygen gas was detected during photocurrent generation in any of these solutions. This means that oxidation of Cl^- ions

dx.doi.org/10.1021/jp209909b | J. Phys. Chem. C 2012, 116, 7612−7620

(eq 3) is the dominant photo-oxidation reaciton that occurs on the WO_3 surface and completely suppresses the O_2 evolution reaction. The generation of Cl_2 gas by photo-oxidation was confirmed by the iodide−starch test, and the test result showed that the majority of photocurrent (>95%) was indeed used for chloride oxidation. The fact that the photocurrents obtained in these solutions did not decay drastically over time suggests that chloride oxidation also effectively suppresses the incomplete water oxidation to peroxo species.[18,19]

Phosphate Solution. Photocurrent−time profiles obtained in 0.1 M NaH_2PO_4 solutions with pH adjusted to 1, 3, and 5 are shown in Figure 5a. (Current−potential characteristics obtained in these solutions are shown in the Supporting Information.) The result shows that photocurrents at all pH conditions were not stable and decreased gradually over time, suggesting the formation and accumulation of peroxide species on the surface of the WO_3 electrode in phosphate solutions.[18,19] Oxygen detection experiments showed that some portion of the photocurrent generated in the phosphate solutions was associated with O_2 production. In Figure 5b, the dashed lines show the expected amount of O_2 calculated from the photocurrent assuming 100% of the photocurrent is associated with O_2 production, while the solid lines show the amount of O_2 that was experimentally detected. The steps or abrupt increase appearing in the solid line in Figure 5b and all other O_2 detection plots shown in this study are due to the abrupt burst of oxygen bubbles that formed and adhered to the Teflon tape above the illuminated spot on the WO_3 photoanode. To ensure that oxygen levels were not under-represented, any remaining bubbles were shaken to burst prior to the final oxygen level reading.

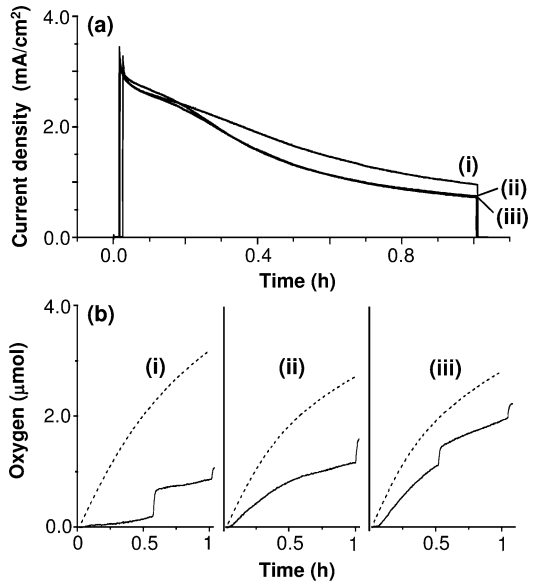

Figure 5. (a) Photocurrent and (b) oxygen measurements of a WO_3 photoanode at 0.9 V vs Ag/AgCl in 0.1 M NaH_2PO_4 solution with pH adjusted to (i) 1, (ii) 3, and (iii) 5 under 400 mW/cm^2 illumination with an AM 1.5G filter. In (b), actual amounts of O_2 produced (−) are compared to expected amounts of O_2 (- - -) calculated from photocurrent assuming 100% photocurrent to O_2 conversion efficiency.

The photocurrent to O_2 conversion efficiencies were 33%, 65%, and 79% at pH 1, 3, and 5, respectively (Table 1). The fact that the photocurrent to O_2 conversion efficiency increases as pH increases suggests that the kinetics of oxygen production increase more rapidly than the kinetics of water oxidation to peroxo species when pH increases. If we assume that the only dominant competing reaction with O_2 evolution in phosphate solutions is the formation of peroxo species, photocurrent obtained in a pH 1 solution should decay the fastest because O_2 evolution was the minimum in this solution. However, all three photocurrents showed comparable decay profiles. This suggests that the amount of peroxo species generated may not be directly related to the amount of peroxo species accumulated on the WO_3 surface resulting in photocorrosion.[18,19] It is also possible that a third competing reaction exists. For example, oxidation of phosphate to peroxydiphosphate was suggested as a possible photo-oxidation reaction that may occur in a phosphate solution in a recent study.[20]

Table 1. Summary of the Photocurrent to Oxygen Conversion Efficiencies Obtained in Electrolytes with Varying pH Conditions and Anions

electrolyte type	pH	photocurrent to oxygen conversion efficiency (%)
CH_3COOH	3	0
CH_3COONa	5	0
NaCl	1	0
NaCl	3	0
NaCl	5	0
NaH_2PO_4	1	33
NaH_2PO_4	3	58
NaH_2PO_4	5	79
$NaClO_4$	1	32
$NaClO_4$	3	29
$NaClO_4$	5	9
Na_2SO_4	1	35
Na_2SO_4	3	63
Na_2SO_4	5	88

Perchlorate Solution. Photocurrents obtained in 0.1 M sodium perchlorate solutions with pH adjusted to 1, 3, and 5 are shown in Figure 6a. (Current−potential characteristics obtained in these solutions are shown in the Supporting Information.) Photocurrents at all pH conditions were not stable and decreased gradually over time, suggesting the formation of peroxide species. Oxygen detection experiments showed that the photocurrent to O_2 conversion efficiencies were 32%, 29%, and 9% at pH 1, 3, and 5, respectively (Figure 6b). These values are much smaller than those obtained from the phosphate solutions. Therefore, if the rest of photocurrent was entirely associated with water oxidation to peroxo species, a faster decay of photocurrent would be expected in the perchlorate solutions than in the phosphate solutions. However, comparison of Figures 5a and 6a revealed that, in fact, the photocurrent decays observed in phosphate and perchlorate solutions are comparable. This again indicates that the amount of peroxo generated may not be directly related to the degree of photocorrosion or that there may be other competing photo-oxidation reactions occurring in the perchlorate solutions. Lewis and co-workers suggested that formation of perchlorate radicals (ClO_4^- $ClO_4(aq) + e^-$, E^o = 2.75 V) is the dominant photo-oxidation reaction in 1 M $HClO_4$ solution and that the perchlorate radical yields O_2 as a final oxidation product.[20] It may be possible that generation of perchlorate radicals may also occur in less acidic solutions (pH 1, 3, 5) used in this study, but its generation and reaction

dx.doi.org/10.1021/jp209909b | J. Phys. Chem. C 2012, 116, 7612−7620

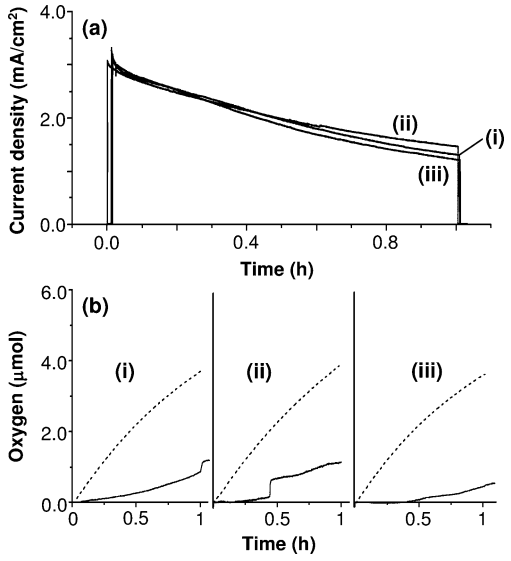

Figure 6. (a) Photocurrent and (b) oxygen measurements of a WO_3 photoanode at 0.9 V vs Ag/AgCl in 0.1 M $NaClO_4$ solution with pH adjusted to (i) 1, (ii) 3, and (iii) 5 under 400 mW/cm^2 illumination with an AM 1.5G filter. In (b), actual amounts of O_2 produced (−) are compared to expected amounts of O_2 (- - -) calculated from photocurrent assuming 100% photocurrent to O_2 conversion efficiency.

pathways may be pH-dependent such that the perchlorate radical does not or only partially yields O_2.

Sulfate Solution. Figure 7a shows photocurrent obtained in 0.1 M Na_2SO_4 solution with pH adjusted to 1, 3, and 5. (Current−potential characteristics obtained in these solutions are shown in the Supporting Information.) Again, photocurrents at all pH conditions decreased gradually over time, suggesting that at least a portion of the photocurrent was

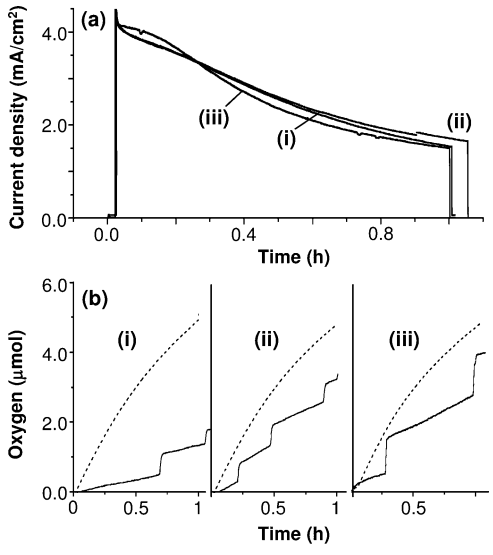

Figure 7. (a) Photocurrent and (b) oxygen measurements of a WO_3 photoanode obtained at 0.9 V vs Ag/AgCl in 0.1 M Na_2SO_4 solution with pH adjusted to (i) 1, (ii) 3, and (iii) 5 under 400 mW/cm^2 illumination with an AM 1.5G filter. In (b), actual amounts of O_2 produced (−) are compared to expected amounts of O_2 (- - -) calculated from photocurrent assuming 100% photocurrent to O_2 conversion efficiency.

associated with the formation of peroxide species. Oxygen detection experiments showed that the photocurrent to O_2 conversion efficiencies were 35%, 72%, and 88% at pH 1, 3, and 5, respectively (Figure 7b). These values are comparable to those obtained in phosphate solutions. However, the decay rates of the photocurrents observed in sulfate solutions (Figure 7a) are slower than those obtained in phosphate solutions (Figure 5a). This is most likely because the holes that were used for peroxo formation in the case of phosphate solutions are now used for both peroxo formation and noncorrosive sulfate oxidation to persulfate, which is another well-known competing photo-oxidation reaction observed in sulfate solutions (eq 4).[18,20] The fact that the photocurrent to O_2 conversion efficiency increases with increasing pH suggests that the kinetics of water oxidation to O_2 improves more rapidly than that of sulfate oxidation or formation of peroxo species when pH increases.

The photocurrent to oxygen conversion efficiencies obtained from various electrolytes discussed above are summarized in Table 1.

Effect of Cations. So far, we have discussed the effect of anions on the photo-oxidation of water by the WO_3 photoanode. However, during our investigation, we observed that the accompanying cations can also affect the photocurrent to oxygen conversion efficiency. One example is shown in Figure 8 where sulfate solutions (pH 3) prepared with lithium,

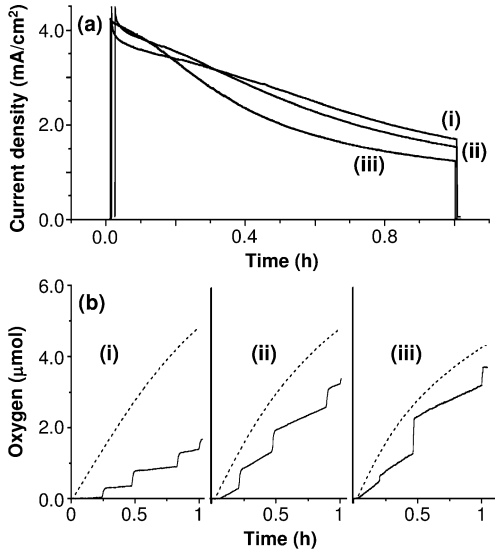

Figure 8. (a) Photocurrent and (b) oxygen measurements of a WO_3 photoanode at 0.9 V vs Ag/AgCl in (i) 0.1 M Li_2SO_4, (ii) 0.1 M Na_2SO_4, and (iii) 0.1 M K_2SO_4 with pH adjusted to 3 under 400 mW/cm^2 illumination with an AM 1.5G filter. In (b), actual amounts of O_2 produced (−) are compared to expected amounts of O_2 (- - -) calculated from photocurrent assuming 100% photocurrent to O_2 conversion efficiency.

sodium, and potassium as the counterions resulted in variation in the photocurrent-to-oxygen conversion efficiencies. The photocurrent to oxygen conversion efficiencies obtained were 35%, 65%, and 80% for Li^+, Na^+, and K^+, respectively. A similar trend was observed with perchlorate and phosphate solutions with the highest photocurrent to oxygen conversion efficiency achieved when using potassium as the counterion (Figures 9 and 10). The photocurrent to oxygen conversion efficiencies

dx.doi.org/10.1021/jp209909b | J. Phys. Chem. C 2012, 116, 7612−7620

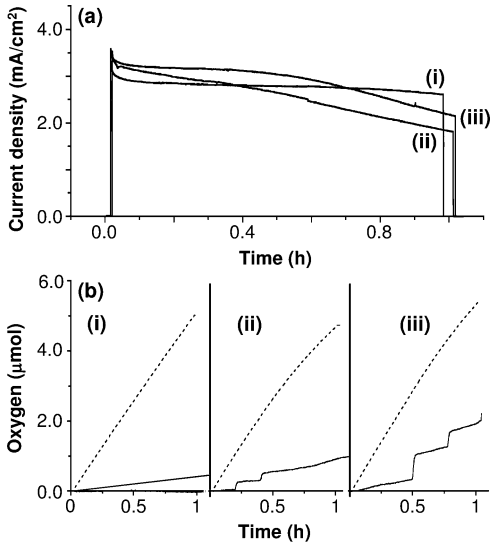

Figure 9. (a) Photocurrent and (b) oxygen measurements of a WO_3 photoanode at 0.9 V vs Ag/AgCl in (i) 0.1 M $LiClO_4$, (ii) 0.1 M $NaClO_4$, and (iii) 0.1 M $KClO_4$ with pH adjusted to 3 under 400 mW/cm^2 illumination with an AM 1.5G filter. In (b), actual amounts of O_2 produced (−) are compared to expected amounts of O_2 (- - -) calculated from photocurrent assuming 100% photocurrent to O_2 conversion efficiency.

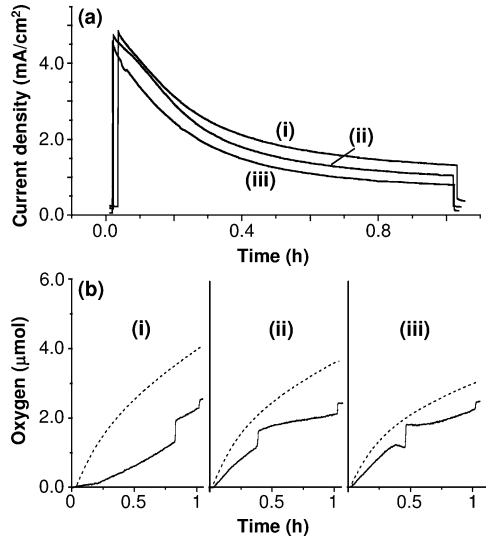

Figure 10. (a) Photocurrent and (b) oxygen measurement of a WO_3 photoanode at 0.9 V vs Ag/AgCl in (i) 0.1 M LiH_2PO_4, (ii) 0.1 M NaH_2PO_4, and (iii) 0.1 M KH_2PO_4 with pH adjusted to 3 under 400 mW/cm^2 illumination with an AM 1.5G filter. In (b), actual amounts of O_2 produced (−) are compared to expected amounts of O_2 (- - -) calculated from photocurrent assuming 100% photocurrent to O_2 conversion efficiency.

for all three electrolytes with varying counterions are summarized in Table 2.

Cations may interfere with O_2 evolution through their adsorption on the WO_3 surface. The point of zero charge of WO_3 is reported to be ca. 0.4−0.5, and, therefore, its surface is expected to be negatively charged at pH 3, allowing for cationic adsorption.[35,36] If the cations adsorb on the active sites for O_2 evolution, it will hinder water oxidation to O_2, and the effect will be more pronounced with higher adsorption strength. It has been demonstrated that the adsorption strength of alkali metal ions on TiO_2 or Fe_2O_3 surfaces is $Li^+ > Na^+ > K^+$.[37] If the same strength of cationic adsorption is assumed for the WO_3 surface, the observed trend for photocurrent to oxygen conversion efficiencies (i.e., the highest photocurrent to O_2 conversion efficiency with K^+ ions and the lowest with Li^+ ions) can be easily explained. Because of the more covalent nature of the interaction between Li^+ ions and terminal oxygen ions on the WO_3 surface, Li^+ ions are expected to serve as a stronger blocker for active O_2 evolution sites and, therefore, reduce the portion of holes used for O_2 evolution in the most effective manner.

Table 2. Summary of the Photocurrent to Oxygen Conversion Efficiencies Obtained in Electrolytes with Varying Cations

electrolyte type	pH	photocurrent to oxygen conversion efficiency (%)
Li_2SO_4	3	35
Na_2SO_4	3	63
K_2SO_4	3	79
$LiClO_4$	3	10
$NaClO_4$	3	29
$KClO_4$	3	49
LiH_2PO_4	3	63
NaH_2PO_4	3	67
KH_2PO_4	3	87

CONCLUSIONS

A high surface area porous WO_3 electrode was prepared by electrodeposition using an aqueous plating solution containing 50 vol % EG. The use of EG allowed for the production of high surface area WO_3 electrodes at an elevated temperature in a more reproducible manner. The resulting n-type WO_3 electrode was used as a photoanode in a water-splitting photoelectrochemical cell. The types of anions (acetate, chloride, phosphate, perchlorate, and sulfate) and cations (Li^+, Na^+, and K^+) contained in the electrolyte as well as pH conditions were varied systematically to investigate how these conditions affect the portion of photogenerated holes used for the O_2 evolution reaction (i.e., photocurrent to O_2 conversion efficiency). The total anodic photocurrents obtained in various electrolytes were comparable, which made it possible to compare the effect of different cations/anions on the selectivity of the photo-oxidation of water to O_2 simply by comparing the photocurrent to oxygen conversion efficiencies. The results show that when acetate and chloride ions are present, the oxidation of acetate and chloride became dominant photo-oxidation reactions, completely suppressing O_2 evolution. When a phosphate solution was used, O_2 evolution and the formation of peroxo species by water oxidation were the two major photo-oxidation reactions. The photocurrent to oxygen conversion efficiency in the phosphate solution was pH dependent, and it increased gradually as pH increases. When a perchlorate solution was used, O_2 evolution and the formation of peroxo species by water oxidation also appeared to occur simultaneously. However, the photocurrent to oxygen conversion efficiencies obtained in perchlorate solutions were much smaller than those obtained in phosphate solution, and they decreased as pH increased. This may indicate the presence of a third competing reaction that is more favored at an elevated pH, possibly oxidation of the reduced species of perchlorate ions generated at the counter electrode. When sulfate solutions were used, photo-oxidation of sulfate to

dx.doi.org/10.1021/jp209909b | J. Phys. Chem. C 2012, 116, 7612−7620

persulfate could also compete with water oxidation to O_2 and peroxo species. When the pH of the sulfate solution increased, the photocurrent to oxygen conversion efficiency increased, indicating that increasing pH improves the kinetics of O_2 evolution more rapidly than the kinetics of peroxo formation or sulfate oxidation. Cations also appear to exert a substantial effect on the photocurrent to O_2 conversion efficiency. In phosphate, sulfate, and perchlorate solutions at pH 3, the highest photocurrent to O_2 conversion efficiency was always obtained with K^+ and the lowest with Li^+ ions. This is most likely because Li^+ ions can adsorb on the WO_3 surface more strongly and serve as a more effective blocker for active O_2 evolution sites. This study, which for the first time discussed the effect of various electrolytes on the efficiency of water oxidation to O_2 in a quantitative manner, will provide a good foundation in formulating optimum electrolyte compositions to enhance the efficiency of desired photo-oxidation reactions for various photoelectrochemical cells.

■ ASSOCIATED CONTENT

Supporting Information

XRD patterns and UV−vis spectrum of WO_3 electrodes, GC result of photo-oxidation of acetate by WO_3, and LSVs obtained with choppped illumination in phosphate, perchlorate, and sulfate solutions. This material is available free of charge via the Internet at http://pubs.acs.org.

■ AUTHOR INFORMATION

Corresponding Author

*Tel.: (765) 494-0049. Fax: (765) 494-0239. E-mail: kchoi1@purdue.edu.

Notes

The authors declare no competing financial interest.

■ ACKNOWLEDGMENTS

This work was financially supported by the Center for Chemical Innovation of the National Science Foundation (Grant CHE-0802907) and made use of the Life Science Microscopy Facility at Purdue University.

■ REFERENCES

(1) Santato, C.; Odziemkowski, M.; Ulmann, M.; Augustynski, J. *J. Am. Chem. Soc.* **2001**, *123*, 10639−10649.
(2) Yang, B.; Barnes, P.; Bertram, W.; Luca, V. *J. Mater. Chem.* **2007**, *17*, 2722−2729.
(3) Santato, C.; Ulmann, M.; Augustynski, J. *Adv. Mater.* **2001**, *13*, 511−514.
(4) Wang, H. L.; Deutsch, T.; Turner, J. *J. Electrochem. Soc.* **2008**, *155*, F91−F96.
(5) Miller, E. L.; Marsen, B.; Paluselli, D.; Rocheleau, R. *Electrochem. Solid-State Lett.* **2005**, *8*, A247−A249.
(6) Cole, B.; Marsen, B.; Miller, E.; Yan, Y.; To, B.; Jones, K.; Al-Jassim, M. *J. Phys. Chem. C* **2008**, *112*, 5213−5220.
(7) Berger, S.; Tsuchiya, H.; Ghicov, A.; Schmuki, P. *Appl. Phys. Lett.* **2006**, *88*, 203119−1−203119−3.
(8) de Tacconi, N. R.; Chenthamarakshan, C. R.; Yogeeswaran, G.; Watcharenwong, A.; de Zoysa, R. S.; Basit, N. A.; Rajeshwar, K. *J. Phys. Chem. B* **2006**, *110*, 25347−25355.
(9) Amano, F.; Li, D.; Ohtani, B. *J. Electrochem. Soc.* **2011**, *158*, K42−K46.
(10) Su, J.; Feng, X.; Sloppy, J.; Guo, L.; Grimes, C. *Nano Lett.* **2011**, *11*, 203−208.
(11) Vidyarthi, V.; Hofmann, M.; Savan, A.; Sliozberg, K.; Konig, D.; Beranek, R.; Schuhmann, W.; Ludwig, A. *Int. J. Hydrogen Energy* **2011**, *36*, 4724−4731.
(12) Cristino, V.; Caramori, S.; Argazzi, R.; Meda, L.; Marra, G.; Bignozzi, C. *Langmuir* **2011**, *27*, 7276−7284.
(13) Hamilton, J.; Byrne, J.; Dunlop, P.; Brown, N. *Int. J. Photoenergy* **2008**, 185479.
(14) Guo, Y.; Quan, X.; Lu, N.; Zhao, H.; Chen, S. *Environ. Sci. Technol.* **2007**, *41*, 4422−4427.
(15) Baeck, S.; Jaramillo, T.; Brändli, C.; McFarland, E. *J. Comb. Chem.* **2002**, *4*, 563−568.
(16) Gerrard, W. *J. Electroanal. Chem.* **1978**, *86*, 421−424.
(17) Baeck, S.; Choi, K.; Jaramillo, T.; Stucky, G.; McFarland, E. *Adv. Mater.* **2003**, *15*, 1269−1273.
(18) Augustynski, J.; Solarska, R.; Hagemann, H.; Santato, C. *Proc. Soc. Photo-Opt. Instrum. Eng.* **2006**, *6340*, U140−U148.
(19) Seabold, J.; Choi, K.-S. *Chem. Mater.* **2011**, *23*, 1105−1112.
(20) Mi, Q.; Zhanaidarova, A.; Brunschwig, B. S.; Gray, H. B.; Lewis, N. S. *Energy Environ. Sci.* **2012**, *5*, 5694−5700.
(21) Liu, R.; Lin, Y.; Chou, L.; Sheehan, S.; He, W.; Zhang, F.; Hou, H.; Wang, D. *Angew. Chem., Int. Ed.* **2011**, *50*, 499−502.
(22) Wong, G.; Ling, Y.; Wang, H.; Yang, X.; Wong, C.; Zhang, J.; Li, Y. *Energy Environ. Sci.* **2012**, *5*, 6180−6187.
(23) *CRC Handbook of Chemistry and Physics*, 81st ed.; CRC Press: Boca Raton, FL, 2000.
(24) Pourbaix, M. *Atlas of Electrochemical Equilibria in Aqueous Solutions*; National Association of Corrosion Engineers: 1974.
(25) Weinhardt, L.; Blum, M.; Bär, M.; Heske, C.; Cole, B.; Marsen, B.; Miller, E. *J. Phys. Chem. C* **2008**, *112*, 3078−3082.
(26) Yamanaka, K. *Jpn. J. Appl. Phys.* **1987**, *26*, 1884−1890.
(27) Shen, P.; Tseung, A. *J. Mater. Chem.* **1992**, *2*, 1141−1147.
(28) Pauporte, T. *J. Electrochem. Soc.* **2002**, *149*, C539−C545.
(29) Meulenkamp, E. *J. Electrochem. Soc.* **1997**, *144*, 1664−1671.
(30) Koch, D.; Woods, R. *Electrochim. Acta* **1968**, *13*, 2101−2109.
(31) Vijh, A.; Conway, B. *Chem. Rev.* **1967**, *67*, 623−664.
(32) Cervino, R.; Triaca, W.; Arvia, A. *J. Electroanal. Chem.* **1984**, *172*, 255−264.
(33) Dickinson, T.; Wynne-Jones, W. *Trans. Faraday Soc.* **1962**, *58*, 388−399.
(34) Fleischmann, M.; Mansfield, J.; Wynne-Jones, W. *J. Electroanal. Chem.* **1965**, *10*, 522−537.
(35) Parks, G. *Chem. Rev.* **1965**, *65*, 177−198.
(36) Xu, Y.; Schoonen, A. *Am. Mineral.* **2000**, *85*, 543−556.
(37) Yates, D.; Healy, T. *J. Chem. Soc., Faraday Trans. 1* **1980**, *76*, 9−18.